ISSN (Print) 1226-1750
ISSN (Online) 2233-6656
Journal of Magnetics 23(1), 93-98 (2018) https://doi.org/10.4283/JMAG.2018.23.1.093

Simulation and Analysis of Magnetic Circuit of Water-cooling Magnetorheological Fluid Transmission Device

Jinjie Ji, Zuzhi Tian*, Xiangfan Wu, and Jin Dou

College of Mechanical and Electrical Engineering, China University of Mining and Technology, Xuzhou, China

(Received 26 December 2017, Received in final form 27 February 2018, Accepted 19 March 2018)

Aiming to solve the problem of magnetorheological transmission heat dissipation, this study designs the magnetic circuit of a water-cooling magnetorheological transmission device based on fundamental electromagnetics theory. Finite element method is used to simulate the magnetic field of the measurement device. Results show that the working magnetic induction can reach 0.56 T when the current is 2.0 A, which can satisfy design requirements. The intensity of magnetic induction in the work space increases with the increase of excitation current and permeability of magnetically conductive material, whereas intensity decreases with the increase of work space size. The thickness and cross-sectional dimension of the guidepost group at the heat-dissipating unit have no significant effect on the intensity distribution of magnetic induction of the entire device.

Keywords : magnetorheological transmission, magnetorheological fluids, water cooling, magnetic field, temperature field, simulation analysis

1. Introduction

Magnetorheological (MR) transmission technology is a novel power transmission technology developed using MR fluid as transmission medium [1-3]. The MR fluid controls magnetic flux mainly by controlling the applied magnetic field strength and changing the apparent viscosity of the MR fluid shear stress [4-6]. When the applied magnetic field strength is continuously changed within a certain range, the continuously changing shear stress that corresponds to the strength of magnetic field can be obtained and stepless control of the torque and the rotation speed can be realized [7]. At present, MR transmission technology is most extensively applied in low-power transmission devices [8, 9]. With the development of transmission technology to high-power direction, the applicability of MR transmission technology also needs to be improved to extend the application range of MR transmission technology [10]. However, the amount of heat generated will increase as the power and temperature of the MR fluid increase. High temperature will significantly influence the performance of MR fluids because the operating temperature of MR fluids usually ranges from −20 °C to 150 °C [11]. Devising effective methods to limit the temperature increase of the MR fluid has become an urgent problem that needs to be solved.

Numerous scholars proposed various solutions to address the abovementioned problems. Dogruoz *et al.* adopted a method of mounting a heat sink on an MR damper housing to improve heat dissipation efficiency [12]. Tian Zuzhi *et al.* employed a method of rotating an MR fluid-variable torque device to force convection between the outer surface of the device and the air to enhance cooling effect [13]. Wang Daoming *et al.* used water cooling through the device within the channel to carry out cooling, but the design of the flow channel was complex [14].

A novel large-slip differential MR transmission device combining MR transmission and water-cooling technology is designed based on this problem. This study designed a magnetic circuit of the device based on electromagnetism theory and used finite element analysis to simulate the simplified 3D magnetic circuit model and determine the influence of the magnetic circuit on the MR fluid transmission device.

2. Design of Magnetic Circuit

MR actuator components of the device structure for material selection, magnetic field strength, and heat dissipation are crucial. The content of the magnetic circuit

*Corresponding author: Tel: +86-13952299638
Fax: +86-0516-83590777, e-mail: tianzuzhi@163.com

design demonstrates that the MR transmission device mainly includes magnetically permeable material and magnetic insulation material. To ensure that the magnetic field lines pass through the magnetic circuit, the magnetic part is generally made of magnetic material and the non-magnetic part is generally composed of non-magnetic material to avoid magnetic leakage.

Figure 1 schematically illustrates the designed magnetic circuit of the MR transmission device based on the structural characteristics of the MR transmission device and the design requirements of the magnetic field. This figure facilitates analysis.

As shown in Fig. 1, the magnetic circuit can be divided into the following 10 parts: 1 for the shell, 2 and 3 for the left side panel, 4 for the flow gap, 5 for the drive plate, 6 for the drive plate, 7 for the MR liquid, 8 for the cylindrical group, 9 for the active connection plate, and 2 and 10 for the right side panel. Among them, 2, 3, 10 is radial magnetic circuit, the rest is axial magnetic circuit.

Based on Ohm's law for magnetic circuit, the magnetic resistance of each part of the magnetic circuit is given as:

$$R_{mi} = \frac{l_i}{\mu_i A_i} \tag{1}$$

where l corresponds to the magnetic circuit length, μ is the permeability of the magnetic circuit material, A represents the cross-sectional area of the magnetic circuit, and i is the number of magnetic circuits.

According to Eq. (1) and considering the size indicated in Fig. 1, the reluctance of each section of magnetic circuit can be obtained as:

$$\begin{aligned}
R_{m1} &= \frac{l_1 + l_2}{\mu\pi(R_1^2 - R_2^2)} \quad R_{m2} = \frac{\ln(R_1 + R_2) - \ln R_3}{2\pi\mu_2 l_2} \\
R_{m3} &= \frac{\ln R_3 - \ln(R_4 + R_5)/2}{2\pi\mu_3 l_3} \quad R_{m4} = \frac{l_4}{\pi\mu_4(R_5^2 - R_4^2)} \\
R_{m5} &= \frac{l_5}{\pi\mu_5(R_5^2 - R_4^2)} \quad R_{m6} = \frac{l_6}{\pi\mu_6(R_5^2 - R_4^2)} \\
R_{m7} &= \frac{l_7}{\pi\mu_7(R_5^2 - R_4^2)} \quad R_{m8} = \frac{l_8}{24\mu_8(S_1 + S_2 + S_3 + S_4)} \\
R_{m9} &= \frac{l_9}{\pi\mu_9(R_5^2 - R_4^2)} \quad R_{m10} = \frac{\ln R_3 - \ln(R_4 + R_5)/2}{2\pi\mu_{10} l_{10}}
\end{aligned} \tag{2}$$

Where S_1, S_2, S_3, S_4 represent the area of the cylinder column.

The magnetic field lines form a closed loop in the magnetic circuit when a coil generates a magnetic field under the action of a current. According to ampere loop theorem, the total magnetic resistance of the magnetic circuit is:

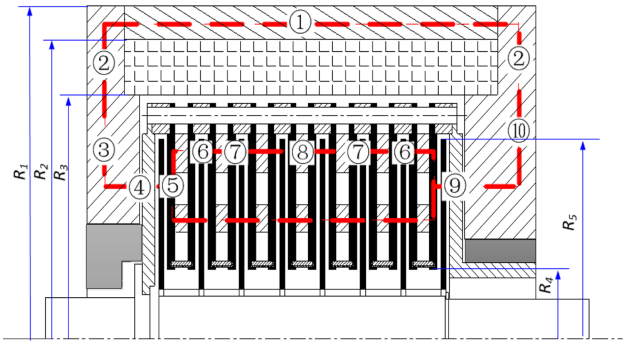

Fig. 1. (Color online) Structure diagram of magnetic circuit.

$$\begin{aligned}
\Sigma R_m = {} & R_{m1} + 2R_{m2} + R_{m3} + 2R_{m4} + 14R_{m5} \\
& + 8R_{m6} + 16R_{m7} + 7R_{m8} + 2R_{m9} + R_{m10}
\end{aligned} \tag{3}$$

The average magnetic flux density of the working gap is known during the design process. According to Gaussian theorem of the magnetic field, the magnetic flux of the working gap is:

$$\Phi = BS \tag{4}$$

According to the basic principle of this road, the magnetic fluxes in all parts of the magnetic circuit are equal when the effect of leakage flux is not considered. The magnetomotive force of the coil can be expressed as:

$$NI = \Sigma R_m \Phi \tag{5}$$

The magnetic circuit reluctance is related to the structure and material of the magnetic circuit. After the total reluctance is determined, the magnetomotive force needed to reach the designed magnetic flux density can be calculated according to Eq. (5). The main parameters of the coil are then determined.

3. Magnetic Field Analysis

ANSYS software using scalar method for magnetic circuit simulation was used to analyze the rationality of the magnetic circuit design. MR transmission components of the material properties can be divided into four categories, wherein the relative permeability of magnetic insulation materials, such as stainless steel, brass, air and cooling water, take an approximate value of 1. In magnetic materials of low-carbon steel, electrically pure iron and MR fluids are nonlinear materials. The magnetically conductive housing of the transmission device, connecting plates, and other transmission plates are made of 20 steel. Magnetic columns are made of pure iron. Magnetorheological (MR) fluid is composed of micro-

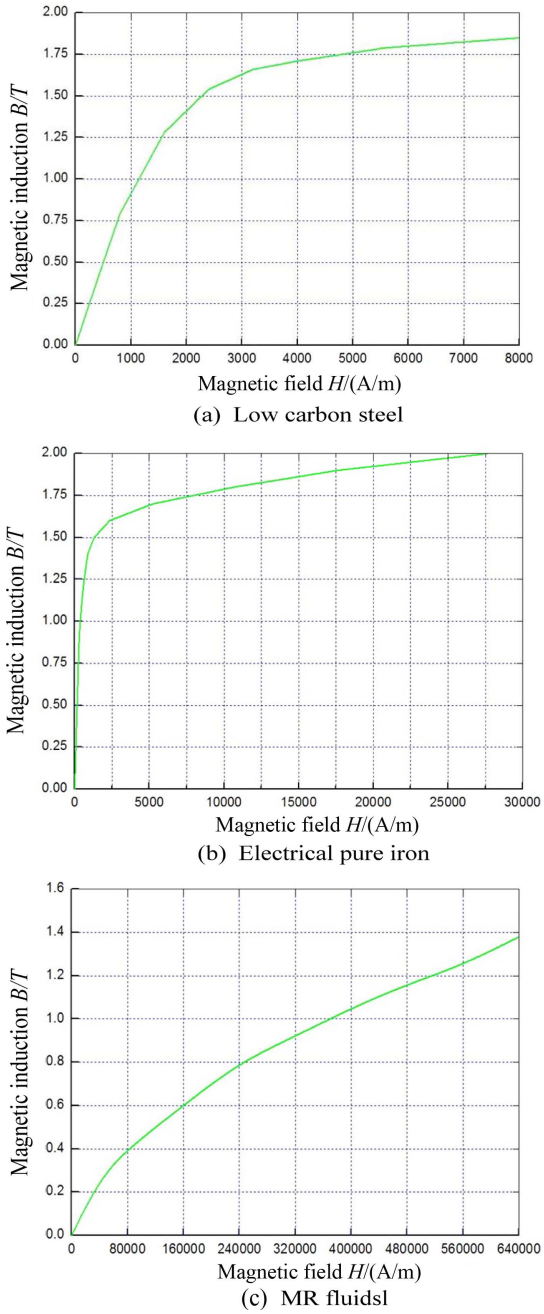

Fig. 2. (Color online) B-H curves of nonlinear materials in magnetic circuit.

sized soft magnetic particles, carrier liquid and stabilizers. Their relative permeability is defined by the BH curve, as shown in Fig. 2.

The 3D finite element model is used for analysis, and the 3D eight-node entity solid96 is used due to the non-symmetrical distribution of the cylindrical group. Figure 3 presents the divided grid.

The current source in the analysis of the 3D scalar method is not a finite element model. Dumbbell unit

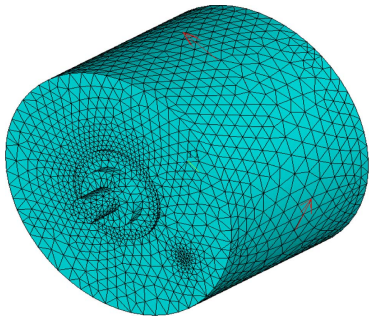

Fig. 3. (Color online) Three-dimensional finite element model.

sourc36 is used to specify the shape, position and the parameters of the current source. In the calculation, one of the geometric points is used to apply the MAG = 0 constraint to avoid the morbid matrix.

3.1. Magnetic field distribution

The total magnetic field distribution of the device with different excitation currents is obtained under the condition of 2400 turns. The half of the cloud is shown in Fig. 4.

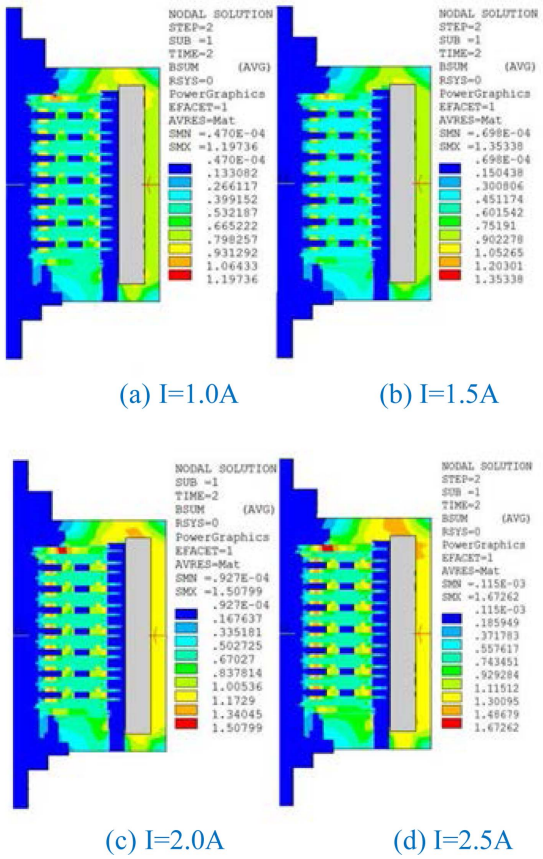

Fig. 4. (Color online) Magnetic induction distribution of MRTD under different currents.

The figure shows that the maximum magnetic induction of the device appears on the active connection disk, which is a phenomenon mainly caused by a considerable change in the reluctance of the magnetic circuit. When the excitation current is 2.5 A, the maximum magnetic field strength is 1.67 T, which is lower than the magnetic saturation strength of the mild steel. When the radius of the main drive disk is small, the large magnetic field intensity is mainly attributed to the small area of the cylindrical group cooperating in this area. The magnetic field lines will be concentrated in such area. The intensity of the magnetic field that passes through the cylindrical group is more intensive than that of the driving disk. The cloud shows that the magnetic field distribution in the working gap is basically uniform. When the excitation current is 2.5 A, the magnetic induction of the working gap can reach 0.6 T, which can satisfy the device requirements for the magnetic field of the working gap, and the magnetic circuit design is basically reasonable.

3.2. Working gap strength of the magnetic field

The effective magnetic field in the MR transmission is only the magnetic field at the working gap. The magnitude of the transmitted torque of the transmission is intrinsically linked to the magnetic field strength at the working gap. The law of the magnetic field distribution along the working gap and the variation law with the field current therefore need to be analyzed. The middle surface of the working gap is difficult to select because of the large number of 3D model nodes of the MR fluid. The magnetic induction intensity is approximated as the magnetic field strength of the working gap for convenient analysis.

The MR transmission device has a multi-disk drive form with eight driven disks. The eight working gaps are located along the power transmission direction to facilitate analysis of magnetic field distribution in the axial gap. The average magnetic flux density distribution of each gap in the axial direction of the device is obtained under the condition of the exciting current of 2.0 A. The number of coil turns is 2400. As shown in Fig. 5, the center of the surface basically has a symmetrical distribution, the magnetic flux density of the working gap at both ends is small, the maximum average magnetic flux density of each gap is only 1 %, and the magnetic flux density is basically uniform in the axial direction.

This analysis demonstrates that the average magnetic field strength of each gap in the axial direction is basically uniform. The fifth driven disk is selected as the study object to obtain a coil to analyze the magnetic flux density distribution of the working gap along the radial direction under different excitation currents. Figure 6 shows the magnetic field intensity distribution along the radial direction under the condition that the number of turns is 2400.

The figure shows that the magnetic induction intensity of the working gap is distributed uniformly along the radial direction. The magnetic induction intensity first increases and then tends to stabilize and then increases as the radius increases. The magnetic circuit model shows that all the driven disks with small radius are all MR fluids. Compared with the low-carbon steel in the magnetic circuit, the lower the MR fluid permeability rate, the greater the reluctance, cylindrical group for the cooling water gap of the main magnetic circuit, with the radius increases, driven disk between the drive plate and cylin-

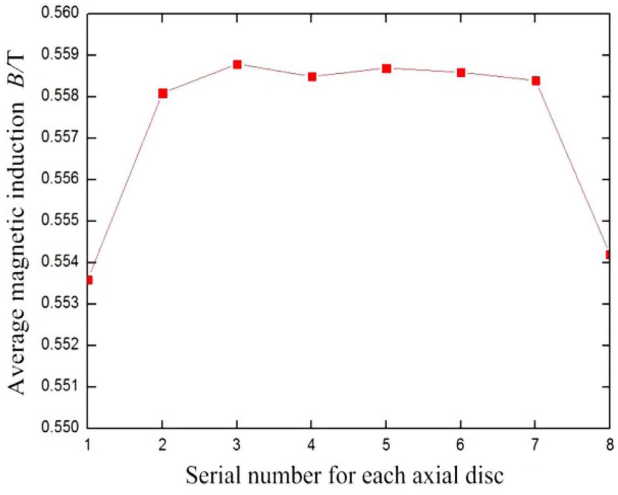

Fig. 5. (Color online) Magnetic induction of $r = 48$ mm on each axial driven plate.

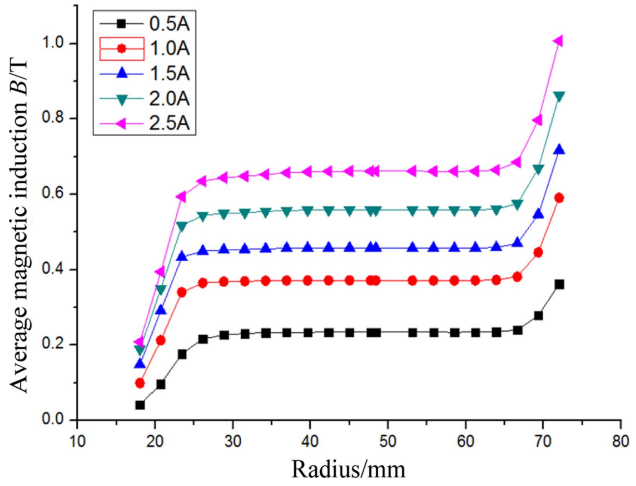

Fig. 6. (Color online) Magnetic induction distribution in radial direction of driven plate.

drical group to reduce reluctance. The magnetic permeability area is large at the maximum radius of the cylindrical group, thereby resulting in low magnetic resistance. This distribution law and the distribution law under different excitation currents is basically the same, and the magnetic field intensity at the working gap increases with the increase of the excitation current.

After determining the main device parameters, the excitation current becomes the main factor that influences the average magnetic field strength of the working gap. The variation of the magnetic flux density with the exciting current in the working gap is obtained to study the relationship between the two factors, as shown in Fig. 7.

The working gap intensity increases with the increase of excitation current. The variation tendency is non-linear, but it decreases gradually as the excitation current increases because the magnetic circuit has non-linear material. The figure shows that the current in the excitation coil allows the design of the magnetic circuit to improve the use of space.

When exciting current meets the working requirements, the relationship between magnetic induction intensity in the working space and working space size is shown in Fig. 8. The main reason is that the total magnetic resistance of magnetic circuit becomes larger as working space size increases. The magnetic induction of driven disk is respectively 0.693T, 0.559T and 0.448T when the working space size h is 1.0 mm, 1.5 mm and 2.0 mm respectively. The corresponding change range of the magnetic induction intensity is 35.4 %.

When exciting current meets the working requirements,

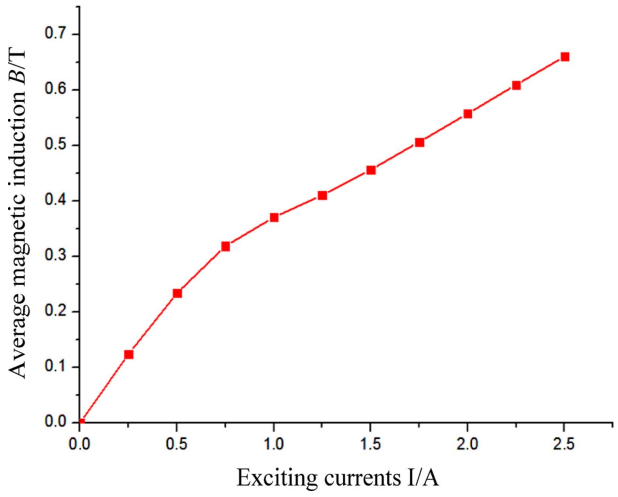

Fig. 7. (Color online) Variation of working magnetic induction with exciting currents.

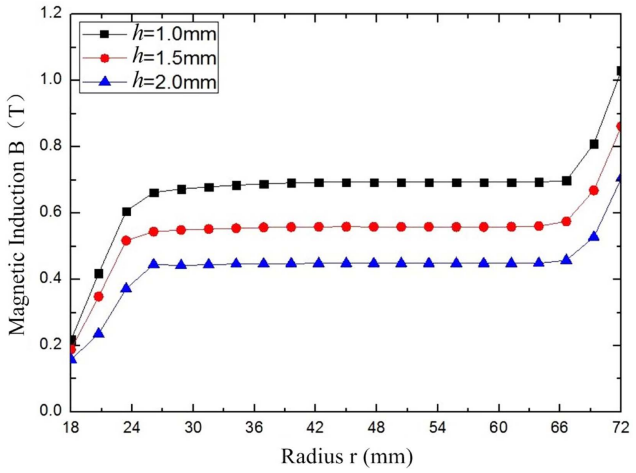

Fig. 8. (Color online) Magnetic induction distribution in radial direction with different working spaces.

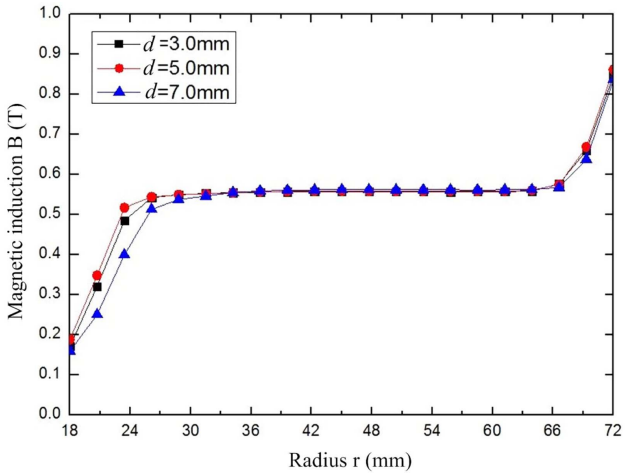

Fig. 9. (Color online) Magnetic induction distribution in radial direction with different thickness of magnetic columns.

the relationship between magnetic induction intensity in the working space and the thickness of magnetically conductive pillar group is shown in Fig. 9. When the thickness of the magnetically conductive pillar group d is respectively 3 mm, 5 mm and 7 mm, the corresponding driven disk at the magnetic inductions is 0.557T, 0.559T and 0.561T. Due to the relatively high relative electrical conductivity of pure iron, with permeability increasing of the column group's thickness, the incomplete distribution of magnetic flux in the working space leads to a slight increase of the magnetic induction intensity, and only 0.7 % of the variation of the magnetic induction intensity. It is considered that the magnetic induction intensity of working space does not change with the thickness of the permeable pillar group.

4. Conclusions

The finite element simulation of the magnetic circuit was performed using the finite element analysis software ANSYS. Results show that the magnetic flux is basically confined in the designed magnetic circuit. The intensity of magnetic induction in the main work space of the driven disk is distributed uniformly in the axial and radial directions. The magnetic flux density of the work space can reach 0.56 T when the excitation current of 2 A. The basic magnetic circuit design can satisfy design requirements. The magnetic induction intensity in the work space increases with the increase of the excitation current and the permeability of the magnetically conductive material and decreases with the increase of the work space size. When work space size h is 1.0, 1.5, and 2.0 mm, the magnetic induction at r = 48 mm of the driven disk is respectively 0.693, 0.559, and 0.448 T, which correspond to a change of magnetic induction intensity at 35.4 %. The thickness and cross-sectional dimension of the guidepost group at the cooling unit influence the magnetic induction intensity distribution of the entire device. The magnetic flux density slightly increases with the increase of the thickness of the magnetically permeable column due to the incomplete dispersion of the magnetic flux in the work space. The variation of magnetic flux density is only 0.7 %. The heat dissipation capability of the transmission can be adjusted by changing the parameters of the magnetic cylindrical group without significantly affecting the magnetic induction intensity in the work space of the transmission.

Acknowledgment

The support of National Natural Science Foundation of China (No.51575512, 51675520, 51405488) the Postdoctoral Science Foundation of China and Jiangsu Province (No.2013M541754 and 1302074C) and the Priority Academic Program Development of Jiangsu Higher Education Institutions in carrying out this research are gratefully acknowledged.

References

[1] S. R. Agustin, F. Donado, and R. E. Rubio, J. Magn. Mater. **335**, 149 (2013).
[2] Y. H. Huang, Y. H. Jiang, X. B. Yang, and R. Z. Xu, J. Magn. **20**, 317 (2015).
[3] H. J. Kim, G. C. Kim, G. S. Lee, T. M. Hong, and H. J. Choi, J. Nanosci. Nanotechnol. **13**, 6005 (2013).
[4] Z. Z. Tian, F. Chen, and D. M. Wang, J. Intell. Mater. Syst. Struct. **25**, 1937 (2014).
[5] X. F. Wu, X. M. Xiao, Z. Z. Tian, and F. Chen, J. Magn. **21**, 229 (2016).
[6] X. F. Wu, X. M. Xiao, Z. Z. Tian, F. Chen, and J. Wang, J. Magn. **21**, 244 (2016).
[7] O. Erol, B. Gonenc, D. Senkal, S. Alkan, and H. Gurocak, J. Intell. Mater. Syst. Struct. **23**, 427 (2012).
[8] X. B. Yang, Y. H. Jiang, Y. H. Huang, R. Z. Xu, H. G. Piao, G. M. Jia, and X. Y. Tan, J. Magn. **19**, 345 (2014).
[9] M. Ashtiani, S. H. Hashemabadi, and A. Ghaffari, J. Magn. Magn. Mater. **374**, 716 (2015).
[10] M. Basili, M. De. Angelis, and G. Fraraccio, J. Sound. Vib. **332**, 3113 (2013).
[11] Z. Z. Tian, C. W. Guo, F. Chen, and X. F. Wu, J. Magn. **22**, 281 (2017).
[12] S. R. Patil, K. P. Powar, and S. M. Sawant, Appl. Therm. Eng. **98**, 238 (2016).
[13] Z. Z. Tian, F. Chen, and D. M. Wang, J. Intell. Mater. Syst. Struct. **26**, 414 (2015).
[14] D. M. Wang, B. Zi, Y. Zeng, Y. F. Hou, and Q. R. Meng, J. Mater. Sci. **49**, 8459 (2014).